




Emergence of surface superconductivity through interference in proximitized topological insulatorsYajiang Chen ^{1,*} Ke-Ji Chen ¹ Jia-Ji Zhu,² and A. A. Shanenko ³¹Key Laboratory of Optical Field Manipulation of Zhejiang Province, Department of Physics, Zhejiang Sci-Tech University, 310018 Zhejiang, China²School of Science, Chongqing University of Posts and Telecommunications, Chongqing 400065, China³HSE University, 101000 Moscow, Russia

(Received 30 January 2024; revised 1 May 2024; accepted 11 June 2024; published 24 June 2024)

Proximitized topological insulators (PTIs) have received significant research attention over the past two decades. In this paper, we demonstrate that a low-dimensional PTI in the topologically nontrivial phase (TP) exhibits interference-induced surface superconductivity (SSC) at the system ends/edges with the critical temperature T_{cs} significantly higher than T_{cb} deep inside the system (low-dimensional bulk). Such an SSC is built due to the interference of the scattering quasiparticle states, rather than the presence of the topological bound states (TBSs). As the system delves deeper into the TP, a nontrivial competition between the scattering quasiparticles and TBSs at the surface leads to a crossover from the interference- to TBS-induced phase, where the SSC is governed by the TBSs. Our paper unveils a substantial variation in the maximal T_{cs} along this crossover, attaining values being twice the maximal T_{cb} of the PTI. Beyond shedding light on the nature of the SSC in PTIs, our paper introduces a tangible method for experimentally manipulating their critical superconducting temperatures.

DOI: [10.1103/PhysRevB.109.224514](https://doi.org/10.1103/PhysRevB.109.224514)**I. INTRODUCTION**

Proximitized topological insulators (PTIs) have been studied intensively in the past two decades, due to the exotic behavior of decoherence-immune topological bound states (TBSs) under various superconducting interactions [1–6]. The point of common interest in the context of PTIs is the Majorana quasiparticles considered as a solid candidate for qubits [7]. It has been predicted that they can appear in the core of an s -wave superconducting vortex [1–3,8], at the nodes of unconventional order parameters [9,10] or at the ferromagnet topological insulator/superconductor interface [11,12]. Moreover, besides Majorana states, the PTIs exhibit an unconventional Josephson effect [13], odd-frequency superconductivity (SC) [14], and coexistence of the TBSs and SC in bismuth and stanene ultrathin films [15,16], etc.

The superconducting properties of PTIs have been investigated in many works [17–23]. In particular, the suppression of the condensate at a PTI interface has been reported [18–21] and confirmed by the observed Andreev spectra [24]. Such a suppression assumes a drop in the superconducting critical temperature T_c . However, the dynamical mean-field theory has shown that a two-dimensional attractive (s -wave) Hubbard model with Rashba spin-orbital coupling and a Zeeman field exhibits an enhanced T_c [25]. Further studies are warranted to reconcile these contradictory findings regarding T_c in PTIs and advance our understanding, paving the way for controllable manipulations of T_c in PTIs.

Recently, an exotic interference-induced surface SC (SSC) in the absence of magnetic fields has been predicted within an s -wave superconducting Hubbard model with a trivial

lattice [26–28], where the surface condensate survives between the bulk T_{cb} and surface T_{cs} critical temperatures ($T_{cs} > T_{cb}$) due to interference of scattering (nonlocalized) quasiparticles. The SSC enhancement $\tau = |T_{cs} - T_{cb}|/T_{cb}$ can go up to about 70% [29,30]. Notice that here, the term “interference” refers to the enhancement of the SSC resulting from the superposition of states spread throughout the whole system, rather than being localized near the boundaries. Then, the following questions arise: Can interference-induced SSC exist in PTIs? If so, does it appear only in the topologically trivial regime, or can it coexist with TBSs? This is of particular importance for low-dimensional PTIs due to pronounced proximity effects.

In the present paper, based on the one-dimensional Su-Schrieffer-Heeger (SSH) model at the half filling [4,5,31–35], we demonstrate that a robust interference-induced SSC can occur in low-dimensional PTIs. Strikingly, it is minor in the topologically trivial phase (TTP) of the SSH chain but extremely pronounced in the topological phase (TP) in the presence of the TBSs. The complex interplay (competition/cooperation) of the interference- and TBS-induced contributions to the SSC can be tuned by the staggering parameter δt . In the TP, the interference-induced SSC predominates as δt approaches zero, while for $\delta t \rightarrow -1$ the TBS-induced SSC prevails. Our results reveal that the maximal T_{cs} in the interference- and TBS-induced regimes of the SSC surpasses the maximal low-dimensional bulk T_{cb} (taken deep in the chain for the standard Hubbard model with $\delta t = 0$) by factors of 1.9 and 2.5, respectively.

II. THEORETICAL MODEL

We investigate the SSH chain deposited on top of an s -wave superconductor [see Fig. 1(a)]. The model Hamiltonian includes the normal SSH term (without

*Contact author: yjchen@zstu.edu.cn

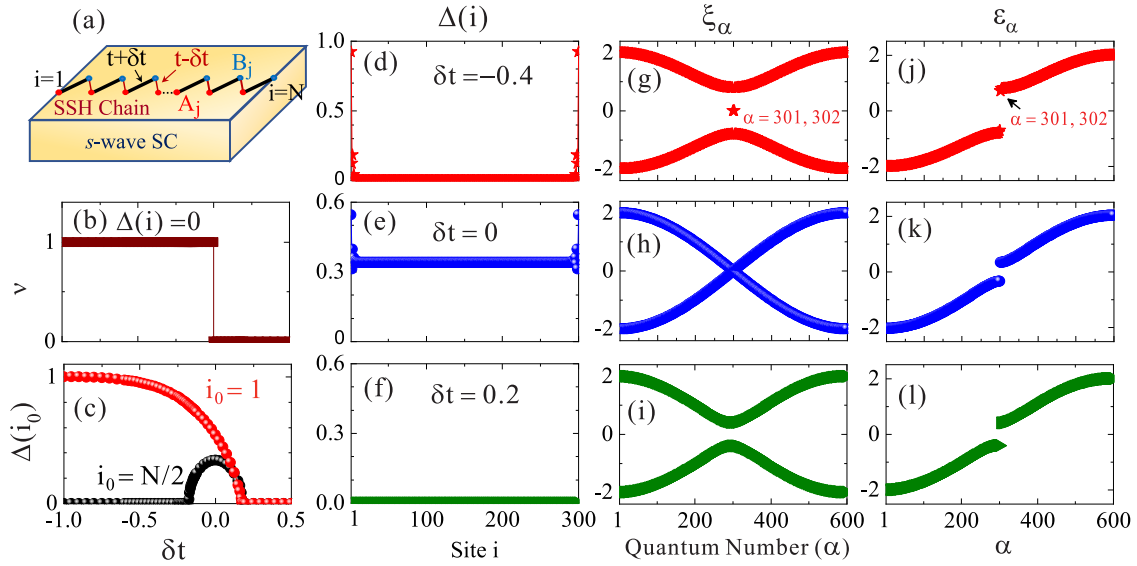


FIG. 1. (a) A proximitized SSH chain. (b) The topological invariant ν as a function of δt without superconducting correlations. (c) The surface (end) and bulk pair potentials, $\Delta_s = \Delta(i_0 = 1)$ and $\Delta_b = \Delta(i_0 = N/2)$, vs δt . (d)–(l) The spatial pair potential $\Delta(i)$ together with the single-electron and quasiparticle energies ξ_α and ϵ_α for $\delta t = -0.4, 0$, and 0.2 at $T = 0$. Only the quasiparticles with $\epsilon_\alpha \geq 0$ (i.e., $\alpha \geq 301$) are physical and contribute to $\Delta(i)$, as displayed in Eq. (2).

pairing) [4,5] $H_0 = -\sum_{j\sigma}(t + \delta t)c_{A_j\sigma}^\dagger c_{B_j\sigma} - \sum_{j\sigma}(t - \delta t)c_{A_{j+1}\sigma}^\dagger c_{B_j\sigma} - \sum_{j\sigma}\mu(c_{A_j\sigma}^\dagger c_{A_j\sigma} + c_{B_j\sigma}^\dagger c_{B_j\sigma})$ and the effective proximitized interaction $H_{SC} = -g\sum_i n_{i\uparrow}n_{i\downarrow}$. Here, the indices $i(=1, \dots, N)$ and $j(=1, \dots, N/2)$ enumerate the chain and sublattice $A(B)$ sites, and an odd (even) i corresponds to the $A(B)$ sublattice; $c_{A(B)\sigma}$ and $c_{A(B)\sigma}^\dagger$ are the annihilation and creation operators of an electron with the spin σ on the sites $A(B)_j$; $n_{i\sigma}$ is the site-dependent electron number operator, $t \pm \delta t$ are the hopping amplitudes in a unit cell and between neighboring unit cells, μ is the chemical potential, and $g(>0)$ is the effective coupling. We recall that the normal SSH chain in the TP with $\delta t < 0$ hosts TBSs and two scattering branches $E_\pm = \pm\sqrt{2[t^2 + \delta t^2 + (\delta t^2 - t^2)\cos k]}$, with k being the dimensionless wave number [5]. For $\delta t > 0$ one gets the TTP with the same E_\pm but excluding the TBSs. Our consideration follows the phenomenological Fu-Kane model [1] where the Cooper-pair tunneling is taken into account by including the s -wave pairing term H_{SC} .

Applying the mean-field approximation $H'_{SC} = \sum_j [\Delta(A_j)c_{A_j\uparrow}^\dagger c_{A_j\downarrow} + \Delta(B_j)c_{B_j\uparrow}^\dagger c_{B_j\downarrow} + \text{H.c.}]$ and diagonalizing the effective Hamiltonian $H_{\text{eff}} = H_0 + H'_{SC}$ [36], one gets the Bogoliubov–de Gennes (BdG) equations

$$\epsilon_\alpha u_\alpha(i) = \sum_{i'} H_{ii'} u_\alpha(i') + \Delta(i) v_\alpha(i), \quad (1a)$$

$$\epsilon_\alpha v_\alpha(i) = \Delta^*(i) u_\alpha(i) - \sum_{i'} H_{ii'}^* v_\alpha(i'), \quad (1b)$$

where $\{\epsilon_\alpha, u_\alpha(i), v_\alpha(i)\}$ are the quasiparticle energies and wave functions, with α enumerating the states in the energy ascending manner, $H_{ii'} = -\sum_{\eta=\pm 1} [t - (-1)^\eta \text{sgn}(\eta)\delta t] \delta_{i', i+\eta} - \mu \delta_{ii'}$, and the pair potential $\Delta(i)$ obeys the s -wave self-consistency relation

$$\Delta(i) = g\langle c_{i\uparrow} c_{i\downarrow} \rangle = g \sum_{\epsilon_\alpha > 0} u_\alpha(i) v_\alpha^*(i) [1 - 2f(\epsilon_\alpha)], \quad (2)$$

with $f_\alpha = f(\epsilon_\alpha)$ the Fermi-Dirac function. At the half filling $\bar{n}_e = \sum_i n_e(i)/N = 1$, with $n_e(i)$ the electron density. This is guaranteed by the self-consistent calculation of the chemical potential μ according to $n_e(i) = 2 \sum_\alpha [f_\alpha |u_\alpha(i)|^2 + (1 - f_\alpha) |v_\alpha(i)|^2]$. Finally, to investigate surface (end) effects, the open boundary conditions are employed for $u_\alpha(i)$ and $v_\alpha(i)$.

Here we note that the mean-field approximation is well justified in our paper, as the SSH chain is coupled to the stable three-dimensional bulk condensate. In this case severe one-dimensional superconductive fluctuations are suppressed by this coupling, as it has been demonstrated in the previous works [37–39].

Below, the energy-related quantities, such as $\Delta(i)$, δt , ϵ_α , and g , are given in the units of the hopping parameter t , while T is in the units of t/k_B , with k_B the Boltzmann constant. The following parameters are used in our calculations: $\bar{n}_e = 1$, $g = 2$, and $N = 300$. The self-consistency convergence accuracy for $\Delta(i)$ is 10^{-12} .

III. RESULTS AND DISCUSSIONS

A. Interference-induced SSC

To begin the discussion of our numerical results, we consider the effects of varying the hopping staggering parameter δt at $T = 0$. The topological invariant ν (the winding numbers) is shown versus δt in Fig. 1(b) for $\Delta(i) = 0$. The topological phase transition occurs at $\delta t = 0$ in the normal SSH model [5] at $\bar{n}_e = 1$ so that the system is in the TP with TBSs for $\delta t < 0$, and in the TTP without TBSs for $\delta t > 0$. The SC in the TP and TTP phases is reflected in the crucial dependence of the pair potential on δt [see Fig. 1(c)], where the end $\Delta_s = \Delta(i = 1, N)$ and bulk $\Delta_b = \Delta(i = N/2)$ are shown versus δt at $T = 0$. One can see that the superconducting correlations disappear when the system goes deep in the TTP while they survive (at the ends) deep in the TP.

Usually, it is believed that only the surface of a PTI is superconducting, so one could expect that the pair potential in the proximitized SSH chain is nonzero only near the chain ends. However, surprisingly, we find that Δ_b can be tuned by δt , as seen from Fig. 1(c). The curve for Δ_b exhibits a dome structure symmetric with respect to the point $\delta t = 0$. We obtain $\Delta_b = 0$ for $|\delta t| \geq \delta t_c = 0.18$ while the maximum of the bulk $\Delta_{b,\max} = 0.34$ is reached at $\delta t = 0$, with the ratio $\Delta_{b,\max}/\delta t_c = 1.89$. This symmetry of Δ_b is directly related to the symmetry of E_{\pm} with respect to the sign change of δt [see discussions above the BdG Eqs. (1)]. At $\bar{n}_e = 1$ the chemical potential μ is located in the gap between E_+ and E_- , which results in large quasiparticle energies ϵ_{α} . When $|\delta t|$ increases, the gap increases together with ϵ_{α} , which results in reducing Δ_b . Finally, it vanishes at $|\delta t| = \delta t_c$. The behavior of Δ_s is remarkably different. For $\delta t > 0$, Δ_s also disappears at $\delta t \geq \delta t_c$. However, for $\delta t < 0$, the dependence of Δ_s on δt changes dramatically due to the appearance of the TBSs affecting the interference of the scattering states near the ends.

Further details about the dependence of our results on δt can be obtained from Figs. 1(d)–1(l). In particular, in Figs. 1(d)–1(f) one can see the site-dependent pair potential $\Delta(i)$ calculated at $T = 0$ for $\delta t = -0.4, 0$, and 0.2 , respectively. In Figs. 1(g)–1(i) one can see the normal-SSH single-particle energy calculated as [40,41] $\xi_{\alpha} = \sum_{i'} u_{\alpha,0}^*(i')H_{i'i}u_{\alpha,0}(i) + v_{\alpha,0}^*(i')H_{i'i}v_{\alpha,0}(i)$ and shown versus α , where $u_{\alpha,0}(i)$ and $v_{\alpha,0}(i)$ correspond to $g = 0$. Our results of ξ_{α} match E_{\pm} (the chemical potential is zero), when taking $k = (\frac{\alpha}{N} - 1)\pi$. Finally, the corresponding quasiparticle energies ϵ_{α} are given in Figs. 1(j)–1(l). Figures 1(d), 1(g), and 1(j) show the results for $\delta t = -0.4$, deep in the TP regime. We find $\Delta_s = 0.924$ while Δ_b is zero. One can see that the single-particle spectrum ξ_{α} contains two branches (E_{\pm}) and four TBSs with $\alpha = 299, 300, 301$, and 302 . However, only the states with positive ϵ_{α} (i.e., the states with $\alpha \geq 301$) are physical and should be taken into account in Eq. (2).

When δt becomes zero, as shown in Figs. 1(e), 1(h), and 1(k), the proximitized SSH model degenerates into the attractive Hubbard model [27,29,30,42]. Here, Δ_b goes up to 0.340 while Δ_s drops to 0.544 , and the gap in the single-particle spectrum ξ_{α} is closed. Finally, deep in the TTP at $\delta t = 0.2$, as shown in Figs. 1(f), 1(i), and 1(l), the site-dependent superconducting correlations disappear both in bulk and at the ends of the chain, and ϵ_{α} approaches $\pm|\xi_{\alpha}|$ (i.e., E_{\pm}). The single-particle spectrum ξ_{α} in Figs. 1(g)–1(i) demonstrates signatures of the topological phase transition, including the opening of the band gap and the appearance of the zero-energy TBSs. However, there are no zero-energy states in the quasiparticle spectrum, as the SSH system with the on-site attraction is not a topological superconductor.

Now, to go into more detail, we investigate the quasiparticle contributions to the end pair potential Δ_s at both the left ($i = 1$) and right ($i = N$) sides of the system. By taking $\delta t = -0.4$ as an example, Fig. 2 illustrates the single-species quasiparticle contributions $\Delta_{\alpha}(i = 1, N)$ to Δ_s at $T = 0$, utilizing the definition $\Delta_{\alpha}(i) = gu_{\alpha}(i)v_{\alpha}^*(i)[1 - 2f(\epsilon_{\alpha})]$. Figures 2(c) and 2(d) are the zoom-in plots of (a) and (b), respectively. The quasiparticle state of $\alpha = 302$ gives the maximal contribution to the SSC at $i = 1$: $\Delta_{302}(i = 1) = 0.494$ with the percentage $\omega_T = \Delta_{302}(i = 1)/\Delta(i) = 53.5\%$. The

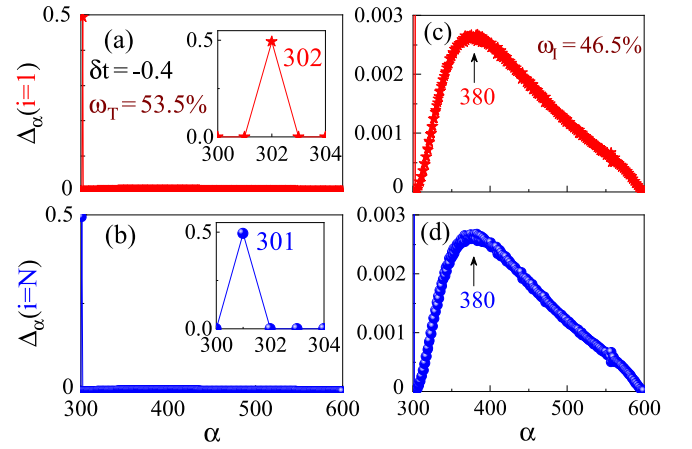


FIG. 2. (a), (b) Single-species quasiparticle contributions $\Delta_{\alpha}(i = 1, N)$ as functions of α for $\delta t = -0.4$ and $T = 0$. The insets and panels (c) and (d) are zoomed-in views of (a) and (b).

single-species contributions of the other states are tiny, e.g., the second largest one comes from the state with $\alpha = 380$, being 0.29% . A similar picture takes place near the right end. The only difference is that the maximal contribution comes from the state with $\alpha = 301$ [see Fig. 2(b)].

It is important to recall that the states with $\alpha = 301$ and 302 for $\delta t = -0.4$ and $T = 0$ have zero single-particle energy, as shown in Fig. 1(g). One can find from Fig. 3 that the wave functions of these states are localized near the chain ends. Thus, the quasiparticles with $\alpha = 301$ and 302 are indeed related to the TBSs of the SSH model. Their inputs to the pair potential $\Delta_{\alpha=301,302}(i)$ are localized near the chain ends [see Figs. 3(a) and 3(d)], so that these states contribute only to the SSC. The remaining quasiparticle states are not bound near the ends, being the scattering states. For example, one can see

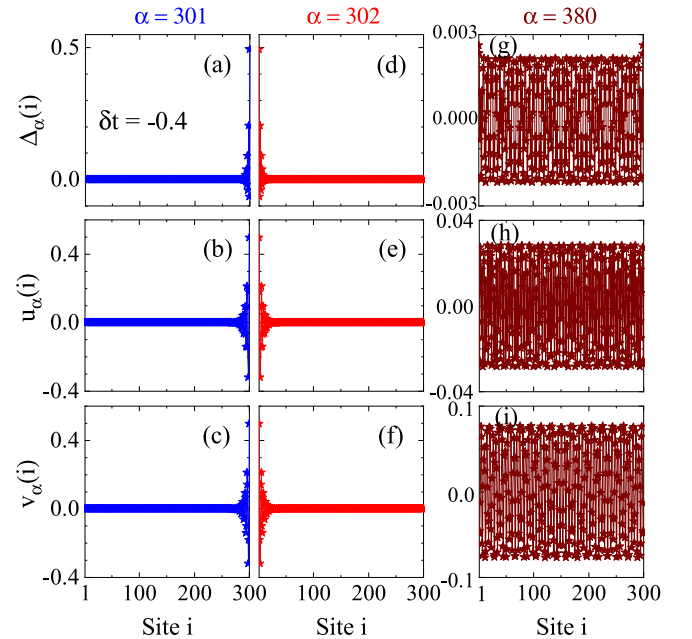


FIG. 3. (a)–(f) $\Delta_{\alpha}(i)$, $u_{\alpha}(i)$, and $v_{\alpha}(i)$ of the topological bound states (TBSs) with $\alpha = 301$ and 302 for $\delta t = -0.4$ at $T = 0$. (g)–(i) The same but for the scattering state with $\alpha = 380$.

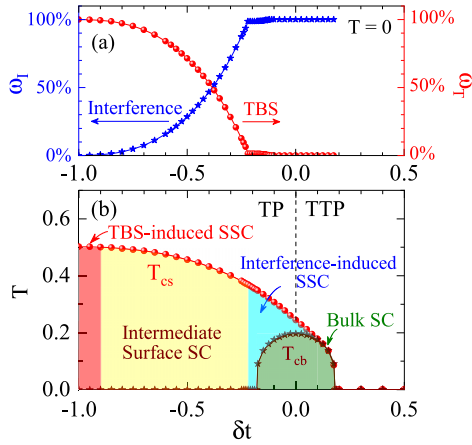


FIG. 4. (a) The contribution percentages of the TBSs and scattering states to $\Delta(i=1)$, i.e., ω_T and ω_I , as functions of δt at $T=0$. (b) The phase diagram of the system in the T - δt plane. The curve with red spheres represents T_{cs} vs δt , and the curve with wine-color stars corresponds to the δt -dependent T_{cb} . The dashed vertical line ($\delta t = 0$) marks the boundary between the TP and TTP.

from Figs. 3(g)–3(i) that the quasiparticle wave functions and the single-species quasiparticle contribution to the pair potential for the state with $\alpha = 380$ are spread all over the chain, with no sign of any localization. However, the constructive interference of all such scattering states produces a significant contribution to the end pair potential [$\omega_I = 1 - \omega_T = 46.5\%$, as seen in Fig. 2(c)] while their destructive interference results in the suppression of Δ_b (see Refs. [27,29,30,42]).

The competition between the interference- and TBS-type contributions to the SSC (i.e., ω_I versus ω_T) is highly sensitive to δt . Figure 4(a) shows ω_I and ω_T as functions of δt for $g=2$ at $T=0$. Both the TBS- and interference-type contributions vary significantly with changing δt . For example, ω_T drops from 100% at $\delta t = -1$ to nearly 1% at $\delta t = -0.22$ while ω_I increases from 0% to almost 99% in the same δt range. Therefore, the interference-induced SSC predominates for $\delta t \geq -0.22$. Near $\delta t = -1$, the system shows the well-known TBS-type SSC. The crossover intermediate regime, with the competing TBS- and interference-induced contributions, is realized for $-0.9 < \delta t < -0.22$.

B. Tunable critical temperatures and phase diagram

Now, we study the upper (surface) and lower (bulk) critical temperatures of the proximitized SSH chain, i.e., T_{cs} and T_{cb} defined by the conditions $\Delta_s(T \geq T_{cs}) = 0$ and $\Delta_b(T \geq T_{cb}) = 0$. Figure 4(b) shows T_{cs} (red spheres) and T_{cb} (wine-color stars) as functions of the hopping staggering parameter δt . The dependencies of T_{cs} and T_{cb} on δt are similar to those of Δ_s and Δ_b at $T=0$ in Fig. 1(c). This implies that the ratios $\gamma_{s,b} = \Delta_{s,b}(T=0)/k_B T_{cs,b}$ are not very sensitive to δt . In particular, we find that $\gamma_b \approx 1.73$, which is close to the case of the conventional BCS superconductors 1.76. In turn, γ_s slightly increases from 2.00 at $\delta t = -1$ to 2.23 at $\delta t = 0$. One can also learn from Fig. 4(b) that T_{cs} and T_{cb} can be controlled and fine tuned by changing δt . In particular, T_{cs} is about 0.50 at $\delta t = -1$, decreases with increasing δt , and

vanishes at $\delta t = \delta t_c$. In turn, T_{cb} is equal to zero for $|\delta t| \geq \delta t_c$ while reaching its maximum 0.20 at $\delta t = 0$.

As seen in Fig. 4(b), the T_{cs} and T_{cb} curves, together with the dashed vertical line $\delta t = 0$ (above the T_{cs}), divide the T - δt plane into four domains with different quantum phases. The nonsuperconducting TTP and TP appear at $\delta t > 0$ and $\delta t < 0$ above the T_{cs} curve, respectively. In these two phases, $\Delta(i)$ equals zero in the entire system, including the bulk and surface regions. The bulk SC phase is located below the T_{cb} curve about $\delta t = 0$ (the dark green region). Finally, the domain of the SSC phase is located between the T_{cs} and T_{cb} curves, where $\Delta(i)$ is nonzero only near the chain edges. Three subdomains can be classified: For $\omega_I \geq 99\%$ we have the interference-induced SSC (the light blue region with $\delta t \geq -0.22$); the TBS-induced SSC corresponds to $\omega_I \leq 1\%$ (the red region with $\delta t \leq -0.9$); the intermediate (crossover) SSC is defined by $1 < \omega_I < 99\%$ (the yellow region with $-0.9 < \delta t < -0.22$). Thus, we arrive at the main conclusion of the present paper: the interference-induced SSC plays a crucial role when the proximitized SSH chain is in the TP regime. Surprisingly, one cannot explain the SSC properties in PTIs only by the presence of the TBSs since the surface constructive interference of the scattering quasiparticles is significant, as well.

C. Possible experimental realization

To experimentally observe our results, one can employ an SSH-type material such as conducting polymers [31,32], e.g., polyacetylene and polythiophene; transition-metal monochalcogenide nanowires, e.g., M_6X_6 ($M = \text{Mo}$ and W ; $X = \text{S}$, Se , and Te) [43–46]; artificial atomic dimer chains made by vacancy sites [47]; and graphene nanoribbons [48,49]. The key controlling parameter (δt) for the SSC crossover and T_{cs} is associated with the energy gap (ΔE_{\min}) between the two non-SC bands of these systems, i.e., $\delta t = \Delta E_{\min}/4$ [31,32,47], which can be tuned by chemical synthesis, doping, strain engineering, etc. Furthermore, according to our numerical results, it is reasonable to expect that other one- and two-dimensional topological insulators under the s -wave superconducting proximity may also exhibit interference-induced SSC and enhanced T_{cs} if the energies of the TBS-related quasiparticles are nonzero. Recall that the zero-energy TBS quasiparticles (i.e., Majorana quasiparticles) are normally hosted in the regions with a suppressed SC.

IV. CONCLUSIONS

The self-consistent numerical BdG calculations for an s -wave proximitized SSH chain have elucidated the emergence of the SSC through the interference of scattering quasiparticle states, rather than due to the TBSs localized near the chain edges. The constructive interference of scattering quasiparticle states results in an enhanced SSC near the chain edges, whereas their destructive interference tends to suppress the bulk SC in the chain center. As the system progresses deeper into the TP by decreasing the hopping staggering parameter, the SSC undergoes a crossover from the interference-dominated regime to the TBS-induced regime. In this crossover, the surface critical temperature (T_{cs})

experiences a significant increase, while the bulk critical temperature remains zero. The maximal T_{cs} coincides with the transition to the TBS-dominated SSC regime. Our findings shed light on the nature of the SSC in PTIs and highlight the potential for experimentally modulating the critical temperatures of these materials.

ACKNOWLEDGMENTS

This work was supported by the Science Foundation of Zhejiang Sci-Tech University (Grant No. 19062463-Y) and was also funded within the framework of the HSE University Basic Research Program.

- [1] L. Fu and C. L. Kane, Superconducting proximity effect and Majorana fermions at the surface of a topological insulator, *Phys. Rev. Lett.* **100**, 096407 (2008).
- [2] J. Chen, W. Xu, Z. Tan, Z. Pan, P. Zhu, Z.-M. Liao, and D. Yu, Superconducting proximity in intrinsic magnetic topological insulator MnBi_2Te_4 -NbN hybrid device modulated by Coulomb blockade effect, *Nano Lett.* **22**, 6484 (2022).
- [3] C. Li, Y.-F. Zhao, A. Vera, O. Lesser, H. Yi, S. Kumari, Z. Yan, C. Dong, T. Bowen, K. Wang, H. Wang, J. L. Thompson, K. Watanabe, T. Taniguchi, D. R. Hickey, Y. Oreg, J. A. Robinson, C.-Z. Chang, and J. Zhu, Proximity-induced superconductivity in epitaxial topological insulator/graphene/gallium heterostructures, *Nat. Mater.* **22**, 570 (2023).
- [4] B. A. Bernevig and T. L. Hughes, *Topological Insulators and Topological Superconductors* (Princeton University, Princeton, NJ, 2013).
- [5] S.-Q. Shen, *Topological Insulators: Dirac Equation in Condensed Matter* (Springer, New York, 2017).
- [6] K. Flensberg, F. von Oppen, and A. Stern, Engineered platforms for topological superconductivity and Majorana zero modes, *Nat. Rev. Mater.* **6**, 944 (2021).
- [7] A. Y. Kitaev, Unpaired Majorana fermions in quantum wires, *Phys. Usp.* **44**, 131 (2001).
- [8] J.-P. Xu, M.-X. Wang, Z. L. Liu, J.-F. Ge, X. Yang, C. Liu, Z. A. Xu, D. Guan, C. L. Gao, D. Qian, Y. Liu, Q.-H. Wang, F.-C. Zhang, Q.-K. Xue, and J.-F. Jia, Majorana mode in vortex core of $\text{Bi}_2\text{Te}_3/\text{NbSe}_2$ topological insulator-superconductor heterostructure, *Phys. Rev. Lett.* **114**, 017001 (2015).
- [9] J. Linder, Y. Tanaka, T. Yokoyama, A. Sudbo, and N. Nagaosa, Unconventional superconductivity on a topological insulator, *Phys. Rev. Lett.* **104**, 067001 (2010).
- [10] R. Roy, Topological Majorana and Dirac zero modes in superconducting vortex cores, *Phys. Rev. Lett.* **105**, 186401 (2010).
- [11] C. W. J. Beenakker, Search for Majorana fermions in superconductors, *Annu. Rev. Condens. Matter Phys.* **4**, 113 (2013).
- [12] Y. Tanaka, T. Yokoyama, and N. Nagaosa, Manipulation of the Majorana fermion, Andreev reflection, and Josephson current on topological insulators, *Phys. Rev. Lett.* **103**, 107002 (2009).
- [13] J. R. Williams, A. J. Bestwick, P. Gallagher, S. S. Hong, Y. Cui, A. S. Bleich, J. G. Analytis, I. R. Fisher, and D. Goldhaber-Gordon, Unconventional Josephson effect in hybrid superconductor-topological insulator devices, *Phys. Rev. Lett.* **109**, 056803 (2012).
- [14] J. A. Krieger, A. Pertsova, S. R. Giblin, M. Döbeli, T. Prokscha, C. W. Schneider, A. Suter, T. Hesjedal, A. V. Balatsky, and Z. Salman, Proximity-induced odd-frequency superconductivity in a topological insulator, *Phys. Rev. Lett.* **125**, 026802 (2020).
- [15] H.-H. Sun, M.-X. Wang, F. Zhu, G.-Y. Wang, H.-Y. Ma, Z.-A. Xu, Q. Liao, Y. Lu, C.-L. Gao, Y.-Y. Li, C. Liu, D. Qian, D. Guan, and J.-F. Jia, Coexistence of topological edge state and superconductivity in Bismuth ultrathin film, *Nano Lett.* **17**, 3035 (2017).
- [16] C. Zhao, L. Li, L. Zhang, J. Qin, H. Chen, B. Xia, B. Yang, H. Zheng, S. Wang, C. Liu, Y. Li, D. Guan, P. Cui, Z. Zhang, and J. Jia, Coexistence of robust edge states and superconductivity in few-layer stanene, *Phys. Rev. Lett.* **128**, 206802 (2022).
- [17] T. D. Stanescu, J. D. Sau, R. M. Lutchyn, and S. Das Sarma, Proximity effect at the superconductor-topological insulator interface, *Phys. Rev. B* **81**, 241310(R) (2010).
- [18] M. Lababidi and E. Zhao, Microscopic simulation of superconductor/topological insulator proximity structures, *Phys. Rev. B* **83**, 184511 (2011).
- [19] A. M. Black-Schaffer, Self-consistent superconducting proximity effect at the quantum spin Hall edge, *Phys. Rev. B* **83**, 060504(R) (2011).
- [20] T. Mizushima, A. Yamakage, M. Sato, and Y. Tanaka, Dirac-fermion-induced parity mixing in superconducting topological insulators, *Phys. Rev. B* **90**, 184516 (2014).
- [21] K. Park, G. Csire, and B. Ujfalussy, Proximity effect in a superconductor-topological insulator heterostructure based on first principles, *Phys. Rev. B* **102**, 134504 (2020).
- [22] Z.-G. Liu, X.-W. Luo, S.-Y. Qin, G.-C. Guo, and M. Gong, Inverse proximity effect in a topological-insulator-superconductor hybrid system, *Phys. Rev. B* **106**, 094501 (2022).
- [23] Q.-G. Zhu and T. Zhou, Proximity effect and inverse proximity effect in a topological-insulator/iron-based-superconductor heterostructure, *Phys. Rev. B* **107**, 094506 (2023).
- [24] P. Zareapour, A. Hayat, S. Y. F. Zhao, M. Kreshchuk, A. Jain, D. C. Kwok, N. Lee, S.-W. Cheong, Z. Xu, A. Yang, G. D. Gu, S. Jia, R. J. Cava, and K. S. Burch, Proximity-induced high-temperature superconductivity in the topological insulators Bi_2Se_3 and Bi_2Te_3 , *Nat. Commun.* **3**, 1056 (2012).
- [25] Y. Nagai, S. Hoshino, and Y. Ota, Critical temperature enhancement of topological superconductors: A dynamical mean-field study, *Phys. Rev. B* **93**, 220505(R) (2016).
- [26] M. D. Croitoru, A. A. Shanenko, Y. Chen, A. Vagov, and J. A. Aguiar, Microscopic description of surface superconductivity, *Phys. Rev. B* **102**, 054513 (2020).
- [27] A. Samoilenka, M. Barkman, A. Benfenati, and E. Babaev, Pair density-wave superconductivity of faces, edges, and vertices in systems with imbalanced fermions, *Phys. Rev. B* **101**, 054506 (2020).
- [28] A. Samoilenka and E. Babaev, Boundary states with elevated critical temperatures in Bardeen-Cooper-Schrieffer superconductors, *Phys. Rev. B* **101**, 134512 (2020).
- [29] Y. Bai, Y. Chen, M. D. Croitoru, A. A. Shanenko, X. Luo, and Y. Zhang, Interference-induced surface superconductivity: Enhancement by tuning the Debye energy, *Phys. Rev. B* **107**, 024510 (2023).

- [30] Y. Bai, L. Zhang, X. Luo, A. A. Shanenko, and Y. Chen, Tailoring of interference-induced surface superconductivity by an applied electric field, *Phys. Rev. B* **108**, 134506 (2023).
- [31] W. P. Su, J. R. Schrieffer, and A. J. Heeger, Solitons in polyacetylene, *Phys. Rev. Lett.* **42**, 1698 (1979).
- [32] A. J. Heeger, S. Kivelson, J. R. Schrieffer, and W. P. Su, Solitons in conducting polymers, *Rev. Mod. Phys.* **60**, 781 (1988).
- [33] H. M. Guo and S. Q. Shen, Topological phase in a one-dimensional interacting fermion system, *Phys. Rev. B* **84**, 195107 (2011).
- [34] Y. Wang, G. Rai, S. Haas, and A. Jagannathan, Edge and corner superconductivity in a two-dimensional topological model, *Phys. Rev. B* **107**, 104507 (2023).
- [35] B. Xing, C. Feng, R. Scalettar, G. G. Batrouni, and D. Poletti, Attractive Su-Schrieffer-Heeger-Hubbard model on a square lattice away from half-filling, *Phys. Rev. B* **108**, L161103 (2023).
- [36] P. G. de Gennes, *Superconductivity of Metals and Alloys* (Benjamin, New York, 1966).
- [37] T. T. Saraiva, P. J. F. Cavalcanti, A. Vagov, A. S. Vasenko, A. Perali, L. Dell'Anna, and A. A. Shanenko, Multiband material with a quasi-1D band as a robust high-temperature superconductor, *Phys. Rev. Lett.* **125**, 217003 (2020).
- [38] A. A. Shanenko, T. T. Saraiva, A. Vagov, A. S. Vasenko, and A. Perali, Suppression of fluctuations in a two-band superconductor with a quasi-one-dimensional band, *Phys. Rev. B* **105**, 214527 (2022).
- [39] A. V. Krasavin, A. S. Vasenko, V. S. Stolyarov, and A. A. Shanenko, Suppression of superconducting fluctuations in multiband superconductors as a mechanism for increasing the critical temperature, *JETP Lett.* **119**, 233 (2024).
- [40] A. A. Shanenko, M. D. Croitoru, and F. M. Peeters, Magnetic-field induced quantum-size cascades in superconducting nanowires, *Phys. Rev. B* **78**, 024505 (2008).
- [41] Y. Chen, A. A. Shanenko, M. D. Croitoru, and F. M. Peeters, Quantum cascades in nano-engineered superconductors: geometrical, thermal and paramagnetic effects, *J. Phys.: Condens. Matter* **24**, 265702 (2012).
- [42] L. Chen, Y. Chen, W. Zhang, and S. Zhou, Non-gapless excitation and zero-bias fast oscillations in the LDOS of surface superconducting states, *Phys. B: Condens. Matter* **646**, 414302 (2022).
- [43] K.-H. Jin and F. Liu, 1D topological phases in transition-metal monochalcogenide nanowires, *Nanoscale* **12**, 14661 (2020).
- [44] M. Nagata, S. Shukla, Y. Nakanishi, Z. Liu, Y.-C. Lin, T. Shiga, Y. Nakamura, T. Koyama, H. Kishida, T. Inoue, N. Kanda, S. Ohno, Y. Sakagawa, K. Suenaga, and H. Shinohara, Isolation of single-wired transition-metal monochalcogenides by carbon nanotubes, *Nano Lett.* **19**, 4845 (2019).
- [45] L. Venkataraman, Y. S. Hong, and P. Kim, Electron transport in a multichannel one-dimensional conductor: Molybdenum selenide nanowires, *Phys. Rev. Lett.* **96**, 076601 (2006).
- [46] L. Venkataraman and C. M. Lieber, Molybdenum selenide molecular wires as one-dimensional conductors, *Phys. Rev. Lett.* **83**, 5334 (1999).
- [47] R. Drost, T. Ojanen, A. Harju, and P. Liljeroth, Topological states in engineered atomic lattices, *Nat. Phys.* **13**, 668 (2017).
- [48] O. Gröning, S. Wang, X. Yao, C. A. Pignedoli, G. B. Barin, C. Daniels, A. Cupo, V. Meunier, X. Feng, A. Narita, K. Müllen, P. Ruffieux, and R. Fasel, Engineering of robust topological quantum phases in graphene nanoribbons, *Nature (London)* **560**, 209 (2018).
- [49] D. J. Rizzo, G. Veber, T. Cao, C. Bronner, T. Chen, F. Zhao, H. Rodriguez, S. G. Louie, M. F. Crommie, and F. R. Fischer, Topological band engineering of graphene nanoribbons, *Nature (London)* **560**, 204 (2018).